An innovative multi-component fluoropolymer-based coating on outdoor patinated bronze for Cultural Heritage: Durability and reversibility

An innovative multi-component fluoropolymer-based coating on outdoor patinated bronze for Cultural Heritage: durability and reversibility

Giulia MASI[*a], Elena BERNARDI[b], Carla MARTINI[c], Ivano VASSURA[b], Luka SKRELP[d], Erika Švara FABJAN[d], Nina GARTNER[d], Tadeja KOSEC[d], Claudie JOSSE[e], Jerome ESVAN[f], Maria Chiara BIGNOZZI[a], Luc ROBBIOLA[g], Cristina CHIAVARI[h]

[a] Dipartimento di Ingegneria Civile, Chimica, Ambientale e dei Materiali, Università di Bologna, Bologna (Italy), giulia.masi5@unibo.it, maria.bignozzi@unibo.it
[b] Dipartimento di Chimica Industriale "Toso Montanari", Università di Bologna, Bologna (Italy), elena.bernardi@unibo.it, ivano.vassura@unibo.it
[c] Dipartimento di Ingegneria Industriale, Università di Bologna, Bologna (Italy), carla.martini@unibo.it
[d] Slovenian National Building and Civil Engineering Institute, Ljubljana (Slovenia), luka.skrlep@zag.si, erika.svara@zag.si, nina.gartner@zag.si, tadeja.kosec@zag.si
[e] Centre de Microcaractérisation Raimond Castaing, CNRS (UMS 3623), Toulouse (France), claudie.josse@ums-castaing.fr
[f] Centre Interuniversitaire de Recherche et d'Ingénierie des Matériaux (CIRIMAT), CNRS, Université de Toulouse, Toulouse (France), jerome.esvan@ensiacet.fr
[g] TRACES Lab, CNRS (UMR5608), Université de Toulouse, Toulouse (France), robbiola@univ-tlse2.fr
[h] Dipartimento di Beni Culturali, Università di Bologna, Bologna (Italy), cristina.chiavari@unibo.it

Abstract

The application of protective coatings for the conservation of outdoor metallic artworks is currently considered the best approach actively employed. This paper focuses on the evaluation of the protectiveness of an optimised fluorosilane (FA-MS) coating with low occupational hazard impact and high inhibition efficiency. FA-MS coating was applied on a typical historical as-cast bronze (Cu-Sn-Zn-Pb), artificially patinated by synthetic acid rain dropping, to simulate natural unsheltered patinas. Subsequently, the patinated bronze was coated by brushing and then artificially aged by synthetic rain dropping. In order to investigate the coating-patina system, a multi-analytical approach was applied including scanning electron microscopy coupled with elemental analysis (FEG-SEM with EDS), microstructural analysis of cross-sections produced by Focused Ion Beam milling (FIB) and X-ray Photoelectron Spectroscopy (XPS). The coating homogenously covered the whole patinated surface producing a transparent layer few µms thick. The weathering solutions were also analysed for the assessment of metallic cations release. FA-MS showed excellent protective performances for the patinated bronze exposed to simulated outdoor conditions. Very high values of inhibiting efficiency in terms of metal release in the weathering solutions (up to 99%) were measured.

[*] Corresponding author. Tel: +39 051 2090361; Fax: +39 051 2090322

e-mail address: giulia.masi5@unibo.it (Giulia Masi)

In order to investigate all the necessary requirements for application in conservation field, the durability of FA-MS was also tested on a real bronze artistic casting, in terms of limiting the alloy composition changes (measured by *in-situ* XRF) over time. A good durability of the coating was observed during the ongoing field exposure test.

Lastly, reversibility of FA-MS was investigated by applying different mechanical cleaning methods, such as brushing and blasting. The reversibility was assessed by the evaluation of the morphology (colour change, surface roughness and optical microscopy) and the composition (SEM-EDS and Py-GC-MS chromatography*)* of the cleaned surfaces. Cleaning by brushing proved to be an efficient method for removing this coating without significantly altering the bronze patina.

Keywords: Fluoropolymer; Protective coating; Atmospheric corrosion; Decuprification; Field tests; Coating reversibility.

1. Introduction

In metal conservation, protective coatings are usually applied to form a barrier against aggressive agents (*i.e.* gas, aqueous solutions or particulate). The features of coatings, environments of exposure and conditions of metallic surfaces at the moment of coating application should be considered when protective treatments are chosen. Furthermore, in Cultural Heritage coatings must fulfil strict requirements, as ease of application, minimal aesthetical impact, protective performance, long-term durability, non-toxicity, reversibility and re-applicability [1]. In recent years, several studies proposed innovative protective coatings with peculiar features, such as organosilane-based [2–9] or eco-friendly coatings [10–13]. The scientific community demonstrated the necessity of finding innovative, protective and non-toxic solutions as alternatives to currently used treatments, as acrylic coatings (Incralac®) and micro-crystalline waxes, which show several drawbacks. In particular, Incralac® product showed a crucial issue linked to the toxicity and health risk [14,15], while micro-crystalline waxes exhibited issues related to short lifetime, poor barrier properties, susceptibility to photodegradation and reversibility problems [16–18].

Few studies [19–21] report on the performance of fluoropolymers for the protection of Cu-based alloys in conservation, even though they show outstanding performance in outdoor applications (durability, chemical resistance, flexibility, low dirt retention, photo-stability and moisture/fungus resistance). One of the most used fluoropolymers is polyvinylidene fluoride (PVDF), containing alternating carbon/fluorine and carbon/hydrogen bonds, that provides chemical inertness, hence a high resistance to environmental degradation. Unfortunately, PVDF exhibited poor adhesion properties on patinated substrates, as interacts with the substrates through very weak Van der Waals forces [22]. To solve this issue, it is usually blended with acrylic or silicon-based polymers [22–24]. In [21], PVDF blended with acrylic coating acted as a strong barrier, providing high corrosion resistance. In another study, a new synthesis process was developed, with acrylic polymer mixed with PVDF during polymerization, producing a fluoro-acrylic mixture on a micro-molecular scale [19]. In addition, as required in conservation, the fluoropolymers could be easily removed using a polar solvent (acetone) [25].

For these reasons, a multi-component fluoropolymer-based coating (FA-MS) was developed to include the fluorocarbon functionality (FA) together with an adhesion promoter: a silane modified poly-methyl-methacrylate (MS). FA-MS resulted as a promising treatment against corrosion of outdoor bronzes [26], considering its low occupational hazard and high inhibition efficiency [27,28].

1.1 Research aim

The aim of this study is to assess the protectiveness of FA-MS in the conservation of outdoor artistic bronze, by comparing the performance of coated and uncoated patinated bronze samples. Bronze patination was performed by accelerated ageing through dropping method. This test well simulates the runoff condition on unsheltered outdoor bronzes and produces representative patinas, as discussed in previous published literature [29–31] and detailed in section 2.2. The same method was applied to age the as-coated samples. Corrosion behaviour was studied by integrating data from both metal release in ageing solutions and surface analyses (SEM-EDS and X-ray Photoelectron Spectroscopy, XPS) of aged coated and uncoated samples. In addition, long-term durability of FA-MS is under investigation on a real quaternary bronze monument exposed outdoor: first results after 9 months of exposure are

reported. Lastly, the reversibility of the studied coating through different mechanical cleaning procedures (brushing and blasting) was evaluated by morphological, microstructural and compositional analysis, being aware that total reversibility is never fully achievable. Therefore, we aim at assessing the degree of removability. To avoid the use of toxic chemicals and solvents commonly used in chemical cleaning, only mechanical methods were tested.

2. Experimental

2.1 Materials

As-cast quaternary bronze (Cu-Sn-Zn-Pb) was supplied by an artistic foundry with the following chemical composition (wt%): 6.9±0.6 Sn; 3.1±0.4 Zn; 2.0±0.9 Pb; traces of Al, P, Mn and Si (Cu to balance). It showed a cored dendritic microstructure, with (α + δ) eutectoids and insoluble Pb globules in the interdendritic areas. Shrinkage microcavities due to cooling during casting were also observed. After SiC polishing (P1000 grade), to simulate the unsheltered exposure of real outdoor monuments, bronze coupon samples (25 mm × 25 mm × 5 mm) were patinated by dropping test for a total Time of Wetness (ToW) of 37 days, following the procedure detailed in [31]. The obtained patina appeared of a homogeneous yellowish-brown colour still preserving the polishing grooves.

The colour coordinates in the CIELab space were: L^*=34±2, a^*=4.2±0.4, b^*=10.7±0.9. Dropping test induced general corrosion characterised by oxidation and preferential release of Cu and Zn from the alloy (Figure 1a) [31].

The obtained patina can be assumed equivalent to that formed after several years in unsheltered outdoor exposure [29,32]. Patinated samples were used as uncoated reference and as substrates for coating application.

Synthesis, preparation and application of the FA-MS coating on the patinated substrates followed the procedure described in our previous work [26]. Subsequently, to obtain a self-assembled single layer, the coating was applied on the patinated samples by brushing. FA-MS produces a homogenous coverage of the substrate, while some heterogeneities are observed from a chemical point of view (Figure 1b): the lighter spots are rich in F element due to segregation of the FA in MS. The measurement of colour coordinates was carried out before, after coating application and after ageing, by a Datacolor D400 spectrophotometer operating with a d/0 measuring geometry, a D65 illuminant, 10° observer, a measure area of ∅ 6.6 mm and specular component excluded (SCE). Measurements were performed in the CIELab space, where each colour is defined by three coordinates: L^*, lightness from 0 (black) to 100 (white) and the chromatic coordinates a^* (+a^* red, -a^* green) and b^* (+b^* yellow, -b^* blue). Total colour change is expressed by the ΔE^* value, calculated through Eq. (1):

$$\Delta E^* = \sqrt{(\Delta L^*)^2 + (\Delta a^*)^2 + (\Delta b^*)^2} \quad (1)$$

For each sample, five measurements in different areas were performed. The ΔE^* values reported were calculated by averaging ΔE^* of three samples.

The application of FA-MS induces a slight colour variation of the surface (ΔE^*=3.2±0.7), due to a decrease in lightness (ΔL^*= -1.7±1.6) and an increase in the yellow component (Δb^*=2.5±0.2), while change on a^* axis is negligible (Δa^*=0.47±0.03). This ΔE^* value corresponds to the most conservative of the two thresholds reported as acceptable in the field of Cultural Heritage (ΔE^* equal to 3 [33,34] or 5 [35,36]).

Figure 1

2.2 Accelerated ageing

Uncoated and FA-MS coated samples were exposed to synthetic acid rain solution by dropping test. Prior to dropping, uncoated surfaces of each coupon were masked by epoxy resin. Thus, only the coated surface (25×25 mm^2) of each sample was directly exposed to rain. At least three samples for each substrate were simultaneously tested.

The synthetic rain (pH ~ 4.3) was prepared according to the composition of natural rains collected during winter months in Bologna [37].

Dropping test consisted in weekly cycles of 3 days dropping/1 day dry/2 days dropping/1 day dry. Two cycles were performed up to a ToW of 10 days per sample. A peristaltic pump dropped the synthetic rain on samples by means of capillary tubes, with a dropping rate of 60 mL/h per sample. During each dropping phase, pH, volume and released metals of the runoff solution were measured. For metal analysis, sampled solutions were acidified with HNO_3 65% suprapur to prevent absorption on the HDPE bottle walls and the formation of metal complexes and stored at 4°C. Cu, Zn and Pb concentrations were analysed by Atomic Absorption Spectrometer (AAS) Perkin-Elmer AAnalyst 400 (with both flame and electrothermal atomization) and Perkin-Elmer PinAAcle 900Z, with Transversely Heated and longitudinal Zeeman background correction. The inhibiting efficiency of the tested coating in terms of metal release (η_M) was calculated according to Eq. (2) as defined in [38]:

$$\eta_M = \left(\frac{M_{sol,NC} - M_{sol,C}}{M_{sol,NC}}\right) \times 100 \qquad (2)$$

where M_{sol}: amount of metal M in the ageing solution (Cu, Zn and Pb in $\mu g.cm^{-2}$); *NC*: uncoated sample; *C:* coated sample.

Moreover, during weathering, mass was measured by digital balance KERN AGB210_4 (repeatability of ±0.1 mg). Mass variations were calculated by the difference between the weight of the coupons prior dropping and their weight after dry phase at different ageing times.

2.3 Characterisation

To chemically characterise the coating, XPS analyses were performed on as-coated and aged coated bronze, using a monochromatised Al Kα (hν = 1486.6 eV) source on a ThermoScientific K-Alpha system, as fully detailed in [26,31]. The X-ray spot size was about 400 μm and the pass energy was fixed at 130 eV. Shirley's method for background subtraction was applied, using Thermo ScientificTM Avantage Software. In this study, the reported results were obtained avoiding preliminary ionic cleaning by Ar^+ sputtering of the surface.

Free surface and cross-sections were observed by scanning electron microscopy (SEM) coupled with Energy Dispersive Spectroscopy (EDS) using a FEG-SEM FEI Helios NanoLab 600i coupled to Aztec Oxford EDS system (SDD detector, WD 4mm). Before SEM observation, to ensure samples conductivity, an amorphous graphite layer (about 10 nm) was sputtered on the samples (Leica ACE 600). In-situ FIB cross-sections were produced by Focused Ions Beam (FIB) milling using Ga^+ ions. A platinum (Pt-C) layer (1 μm) was first laid down for surface protection, prior FIB milling. Representative areas were chosen after detailed surface observation, producing cross-sections from 100 to 130 μm in length. SEM and EDS analyses were carried out using an acceleration voltage of 10 kV.

2.4 Field test on durability

In March 2017 a quaternary bronze statue representing the Slovenian poet France Prešeren was exposed outdoors in the park of the Slovenian National Building and Civil Engineering Institute (ZAG) in Ljubljana, to monitor the long-term durability of FA-MS. The statue has the following composition (wt%): 5.7±0.08 Sn, 5.1±0.10 Zn, 1.96±0.14 Pb, 0.27±0.02 Fe (Cu to balance). Before coating application (performed on April 2018), the statue was left to naturally age for a year to allow the formation of natural patinas. The chemical composition of the FA-MS applied on the statue is monitored over time by XRF (Portable XRF Niton, USA; energy applied = 45 kV, Niton XL2 - Ag anode; calibration with reference material CURM No.71.31-5, Leaded Gunmetal, BAS) in three different positions of the statue (∅ of the spots=8 mm): point A-right shoulder, point B-left shoulder, point C-top of the head (Figure 2). The "before" condition corresponds to the as-applied FA-MS on the one-year aged statue, while the "after" condition corresponds to the coated statue exposed for 9 months.

Figure 2

2.5 Reversibility of FA-MS coating

Only a mechanical approach was considered here to assess the reversibility performance of FA-MS applied on patinated bronze. Three cleaning methods were selected among the cheapest and simplest ones applied in field on real monuments: automatic brushing with nylon or steel brushes (10000 rpm) and blasting with glass microsphere beads (100 µm diameter, pressure=2 atm). The cleaning treatments were applied both on as-coated and aged coated samples (paragraph 2.2) and were carried out by a trained restorer.

Before and after cleaning, morphological and microstructural observations were carried out using a 3D-Digital microscopy and a Scanning Electron Microscope (SEM, Carl Zeiss EVO 50) equipped with an Oxford Instrument INCA X-Act Penta-Fet Precision Energy Dispersive Spectroscope (EDS), respectively, using an acceleration voltage of 20 kV. Stylus profilometry (radius of curvature of the stylus tip = 5 µm, precision: 0.2 µm) was performed and the average roughness (Ra) and the root mean square roughness (Rq) values are reported. Colour variation measurements were also carried out on the aged coated samples before and after the cleaning procedure by brushing, following the experimental procedure previously detailed (section 2.1).

Lastly, to develop a semi-quantitative method to assess the efficiency of cleaning treatments, a Pyrolysis-Gas Chromatography-Mass Spectrometry (Py-GC-MS)-based procedure was tested on as-coated samples, uncleaned or cleaned by nylon and steel brushes. An equal spot (0.5 cm x 1 cm) was selected on uncleaned and cleaned coated areas and homogeneous scraping of the surface in each spot was performed with a stainless steel scalpel to reveal the bare alloy. The scraped material was quantitatively transferred in a quartz tube filled with quartz wool and pyrolysed at 600°C for 60 s at the maximum heating rate using a Pyroprobe CDS 5250 connected to a Shimadzu GC-MS-QP2010 equipped with a ZB-35 GC Column (30 m x 0.25 mm, film thickness 0.25 µm). Helium was used as carrier gas (0.93 mL/min) and pyrolysis products were injected in the GC column with a 10:1 split ratio. Both the pyrolysis-GC interface and injector were kept at 270 °C. The temperature of the column was varied from 50˚C to 290˚C with

a heating ratio of 3.70˚C/min until 190 °C were reached, then of 20˚C/min. Peaks were identified according to the NIST11 library and those related to the coating were compared between the different samples.

3. Results and discussion

3.1 Accelerated ageing on uncoated patinated bronze

Compared to natural corrosion of the ongoing field test on bronze after one year exposure (Figure 2 on the left), the dropping test induced extensive surface corrosion (Figure 3). Optical observation (Figure 3a) reveals a non-homogenous distribution of the corrosion products (Figure 3a), marked by an important colour variation from the patinated initial state (ΔE^*=12±1 mainly linked to a lightness variation ΔL^*=11.5±0.6). According to [30], the dropping ageing can be assumed representative of outdoor corrosion on unsheltered areas after at least one decade. As pointed out in [31], dendrites suffered severe corrosion inducing numerous crackslocated in the Cu(Sn) α-phase of the dendrites (Figure 3b), leaving unaffected the delta rich-tin phase of eutectoid in interdendritic areas (Figure 3c). X-ray maps in Figure 3c highlight Sn-enriched corrosion products within the attacked alpha phase: dropping facilitates Cu leaching rather than the precipitation of Cu-based corrosion products [30,31].

Figure 3

Cross-sections obtained by FIB milling and observed by SEM confirm the non-attack of the eutectoid δ-phase and reveals uneven corrosion within the Cu α-phase (Figure 4a). Near to the eutectoid, the dendrite border has a thick (< 5 µm) corrosion layer (Figure 4b), exibitng a two-layer structure marked by a very thin internal layer (< 300 nm) with nanoporosities below a compact outermost one. As shown in X-ray maps (Figure 4d), the corrosion layer is characterized by an enrichment of O and a marked dissolution of Cu, inducing a relative enrichment in Sn. This has to be attributed to decuprification process of bronze in aqueous environments [31,32,39–41]. Within the core of the dendrites, corrosion is characterised by a thick (1-2 µm) internal nano-porous layer below an outermost surface partially flaked (Figure 4c). This nanoporosity of corrosion layer, markedly more pronounced in the core than in the border of the dendrites, is directly related to the corrosion attack and decuprification, which is more significant in the core parts.

Figure 4

3.2 Protectiveness of FA-MS on patinated bronze

3.2.1 Mass variation and metal release

The gravimetric measurements (Figure 5) show the cumulative mass variation (mg/cm^2) as a function of ToW. For the uncoated bronze, an almost linear (R^2=0.967) trend of mass decrease was highlighted, down to -1.4±0.3 mg/cm^2, confirming the morphological surface features. Conversely, coated samples showed a very limited mass variation: a slight mass increase (0.17±0.03 mg/cm^2) was measured since the beginning of the ageing test (ToW=3 d) and

remained nearly constant as a function of exposure time. This could indicate the formation of corrosion products for short ToW or an interaction between the coating and the weathering solution: some water molecules could be trapped within the polymer.

Figure 5

Regarding cation release measurements (Table 1), the uncoated sample shows that Cu, Zn and Pb release increased with exposure time, following a relatively linear trend. In particular, the Cu/Zn ratio of 20 is comparable to the Cu/Zn measured in the alloy (~28), highlightings that Cu and Zn have a similar tendency of dissolution under runoff conditions as also highlighted in [30, 32, 41]. Conversely, the Cu/Pb ratio (~44 in the alloy) linearly increased from 8 to 17 during the ageing. Pb preferentially dissolved compared to Cu, with higher dissolution rate at the beginning of the test, as highlighted in [30]. These results confirm that runoff inhibited the formation of a protective layer of Cu-based corrosion products.

Regarding the coated bronze, a low dissolution rate for Cu, Pb and Zn was recorded, showing excellent barrier properties for FA-MS. The high protectiveness is confirmed during 10 days of dropping test, as demonstrated by the calculation of the inhibiting efficiency η (eq. (1)): 99% (relative standard deviation, rsd=22%) for η_{Cu} and 99% (rsd=15%) for η_{Pb}.

Table 1

3.2.2 XPS analysis of FA-MS coated samples

Concerning the chemical characterisation of the coating, XPS core levels of the main elements were recorded before and after ageing. Table 2 reports the values of XPS peak positions and atomic quantification before and after the dropping test with an accuracy around 10% [42].

Table 2

It is important to mention that the alloying elements (Zn, Sn and Pb) were never detected. Only Cu 2p was detected in traces (<0.1 at%), likely indicating contamination induced by sample preparation. The comparison of XPS results, reported in Table 2, confirms the slight impact of ageing on the FA-MS surface: no remarkable differences in atomic concentrations of the detected elements were observed before and after dropping, except for C 1s and F 1s. In particular, for the oxidised C species and F element, the measured variation is probably linked to the chemical heterogeneity of the FA-MS coating, as shown in Figure 1b and discussed in a previous study [26]. Therefore, the weathering solution did not induce signicant modification in the coating under dropping conditions.

Regarding the C 1s region, a first intense peak at BE=284.7 eV was attributed to C-C and C-H bonds and a shoulder between BE=285.7 eV and BE=286.3 eV is representative of C-O or C-N [43–45]. The contributions characteristic of C=O / O=C-O and CF are located between BE=287.1 eV and BE=289.0 eV, while BE = 291.4 eV and BE=293.8 eV represent CF_2 and CF_3 bonds, respectively [46]. F 1s in turn showed a main peak centred at BE=688.7 eV, attributed to F bound to the organic matrix of the polymer [46], while N (N 1s, BE=400.0 eV, N-C) showed a similar concentration (~ 3 at%) before and after ageing. Si 2p, centred at 101.9 eV, was attributed to the Si-O-Si and/or C-

SI-O bonds [43–45,47,49] of the MS polymer [26]. As expected, MS is mainly responsible of the binding mechanism on bronze substrate through the formation of metal-thiolate bonds, mainly involving Cu and Sn (the latter with minor extent) [8,26,45].

3.2.3 FIB Cross-sections and colour measurements

Cross-section FEG-SEM micrographs and X-ray maps of FA-MS coated patinated bronze, analysed after dropping test, are reported in Figure 6. Figure 6a-b describe the coating morphology, showing no evidence of corrosion attack, as also reported in [26]. The cross-section observation excludes the formation of corrosion products during ageing, suggesting that the mass increase observed in Figure 5 is mainly related to the interaction between coating and weathering solution.

The evidence of no corrosion attack is also confirmed by colour variation measurements (as-coated samples as references). Only a very slight colour variation was induced by accelerated ageing: $\Delta E^{*}=0.65 \pm 0.02$. This value is well below the thresholds reported as acceptable in the field of Cultural Heritage [33–36], and also lower than 1, that represents the just noticeable colour difference in a person with normal colour vision [35,53].

The FA-MS layer is quite thin (2 μm) but homogenously covers the whole patinated surface. In general, the coating appears to be basically undamaged, adherent and homogeneously thick even after ageing, affording excellent protection of the substrate (as demonstrated by metal release and inhibiting efficiency data in §3.2.1). Some infrequent defects were observed, such as a few micro-sized pores (Figure 6c). Moreover, X-ray maps (Figure 6c) confirmed that the coating consists of C, O, F and Si, with some composition heterogeneities, namely F enrichment in the internal layer, near the interface with bronze patina. This effect is linked to coating preparation, indicating that the blending procedure of FA and MS components should be optimised.

Figure 6

3.3 FA-MS durability in field

In-situ XRF measurements were carried out to evaluate the durability of FA-MS in terms of coating ability to preserve the bronze chemical composition. The three measuring points represented unsheltered areas of the bronze statue exposed to natural runoff. XRF measurements show that no significant changes of the bronze chemical composition were detected after 9 months of natural outdoor exposure (Table 3). This indicates that FA-MS well protects the patinated bronze surface. Measurements are still ongoing and will be repeated over longer exposure times.

Table 3

3.4 Reversibility of FA-MS coating from patinated substrates

The assessment of the FA-MS ability to be removed was evaluated using three different mechanical cleaning methods according to restoration practice. Regarding the evolution of the surface morphology, optical microscopy and surface roughness measurements were performed (Figure 7, Table 4).

Figure 7

Specifically, the application of blasting by glass microspheres strongly modified the surface (Figure 7), where microsphere repeated indentation traces are evident. This phenomenon is also highlighted by surface roughness measurements (Table 4) where both Ra (average roughness) and Rq (root mean square roughness) values showed a remarkable increase in coated samples, both in as-coated and coated after ageing conditions. Rq value increased 2.5 times for as-coated samples and more than 4 times for FA-MS after ageing. Thus, this cleaning method detrimentally impacts on the coated surface, inducing the removal of coating but strongly modifying the surface morphology of the bronze, making this method not suitable. Conversely, brushing seems to be a more suitable strategy, even if differences between the use of nylon and steel brushes can be observed, *i.e.* more relevant changes of coated surface morphology for samples cleaned by steel brushes (Figure 7), which allow a more efficient removal of the coating by comparison to nylon which carries out only a partial removal of the polymeric layer (dark areas in SEM images of Figure 8c,g). These features are confirmed by the surface roughness profiles (Figure 7) and by Ra and Rq values reported in Table 4. No significant variation in surface roughness was measured in the sample cleaned by the nylon brush, while a slight decrease was recorded for the steel brush, when compared with the reference samples (as-coated and aged coated before cleaning).

Table 4

SEM micrographs better highlight the impact of the tested cleaning methods (Figure 8). Both as-coated and aged samples after cleaning showed similar behaviour. Regarding blasting by glass microsphere (Figure 8b,f), the dendritic microstructure is not observable anymore and the microsphere indentations are visible on the surface. This confirms the results previously discussed. Nylon brush cleaning seems only partly remove the coating, in fact, with respect to their reference (Figure 8a,e), on both the samples only a slight and scattered enhancement of the contrast of BSE image (Figure 8c,g) is visible. Conversely, the application of steel brush induced more uniform cleaning of FA-MS. This is evident in Figure 8d,h, where the dendritic structure is highlighted without significant traces of the coating.

Figure 8

EDS data before coating and before and after cleaning (with different methods) are compared in Figure 9, considering both the coating (C, O, F and Si, Figures 9a,c) and the alloying elements (Cu, Zn, Sn and Pb, Figures 9b, d). Regarding the coating elements compared to nylon brush, the application of glass beads or steel brush decreased markedly the C and O contents, confirming the better performance of these two methods on both the as-coated and aged coated samples. For the other characteristic elements, a clear trend is not observable, since O is one of the constituents of the patina, while F and Si elements are in low concentrations. In addition, related to alloying elements, when glass blasting and steel brushing were performed, a remarkable increase in Cu and a slight one in Zn and Sn were recorded, making surface composition more similar to that of the patina (before coating). However, glass beads were already ruled out due to the aggressiveness towards surface features as demonstrated by SEM observations and roughness measurements. Steel brush showed better results, due to a higher efficiency in removing the coating without strongly modifying the patina. These results confirm the previous data about surface roughness and morphology (Figures 8-9; Table 4), making steel brushing the most effective cleaning method among the tested ones. The ability of steel

brushing to induce a less perceptible colour variation of the patina after removal of the aged coating is also demonstrated by ΔE^* values: 4.8 for steel vs. 8.8 for nylon brushing.

Figure 9

The high effectiveness of the brush methods in coating removal, especially when steel brush is used, is further confirmed by Py-GC-MS, that also proved to be an effective technique to assess the efficiency of cleaning treatments. The chromatogram of the as-coated surface (Figure 10a) shows two peaks related to fragments containing Si and therefore clearly deriving from the coating: one at 4.9 min, corresponding to propyl trimethoxysilane, the other at 24.0 min, corresponding to (trimethoxysilyl)propyl ester. As the latter is 15 times more intense, it was selected as marker of the coating. In the case of the as-coated surface cleaned with nylon brush, the marker peak shows an intensity decrease of about 95% (Figure 10b), while it results no longer detectable in the case of steel brush cleaning (Figure 10c). explain this result. Considering the performance of nylon brush, it has to be taken into account that Py-GC-MS analyses were performed on the material scraped off a surface area of 0.5 cm^2 (see section 2.5), while SEM EDS maps were recorded over 0.45 mm^2 areas. Hence, Py-GC-MS analyses give a more global result in terms of removability, while EDS maps allowed to highlight the localised distribution of the residual coating (~5 %). Therefore, the general performance of the nylon brush in removing the coating is actually better than previously suggested by localised EDS analyses alone.

Figure 10

4. Conclusions

The following conclusions can be drawn from this study:

- Accelerated ageing by dropping of uncoated patinated bronze induced extensive corrosion, showing a strong colour variation and a corrosion layer with non-homogenous thickness, containing corrosion products with a relative Sn-enrichment. These characteristics were observed also in outdoor patinas of unsheltered areas. Internal cracks within the corrosion layer were detected in the Cu(Sn) dendrites, while the interdendritic spaces with eutectoid were poorly affected. The patina exhibited a two-layer structure, due to selective dissolution of Cu cations and relative Sn enrichment, more pronounced in the external layer than in the internal thinner one. Centres of dendrite were more corroded and exhibited a thinner corrosion layer than their border, due to the rain leaching effect inducing a thinning of the external corrosion layer.
- The application of FA-MS produced a continuous coating of 2 μm on patinated bronze, with very few porosities. This coating induced a very slight colour variation, in the range of acceptability for Cultural Heritage applications. For this reason, FA-MS represents a promising treatment regarding the aesthetical aspect.
- The assessment of the protectiveness of FA-MS through dropping test showed its high inhibiting efficiency (η_M) in terms of Cu and Pb release in the weathering solution. Moreover, Zn was under the limit of detection, indicating that FA-MS coating could inhibit Zn dissolution under the tested conditions. These results were confirmed by XPS analysis and cross-sections observations.

- *In-situ* XRF measurements carried out on a real bronze monument coated with FA-MS and exposed outdoor exhibited no variation of the chemical composition of the surfaces after 9 months of natural exposure. The field monitoring of the long-term durability of the coating is still ongoing.
- Cleaning by brushing was able to remove FA-MS, ensuring the reversibility property, necessary requirement for coating selection in conservation. On the basis of the obtained results, these cleaning methods seem to efficiently remove FA-MS without strongly modifying the morphology and the microstructure of the patinated bronze. Further investigations are planned to confirm this point.

Acknowledgements

This research was performed within the scope of M-ERA.NET European B-IMPACT project (www.b-impact.cloud) and funded by National funding organization from Italy (MIUR), Slovenia (MIZS) and France (RMP). The authors would acknowledge Livartis d.o.o. (Slovenia) for producing bronze coupons and the bronze statue (www.livartis.si/en) and the restorer Ms. Florence Caillaud for performing the cleaning tests.

5. References

[1] D. Watkinson, Preservation of Metallic Cultural Heritage, in: Shreir's Corros., Tony, J.A., Elsevier: Oxford, 2010: pp. 3307–3341.

[2] C. Rahal, M. Masmoudi, M. Abdelmouleh, R. Abdelhedi, An environmentally friendly film formed on copper: Characterization and corrosion protection, Prog. Org. Coatings. 78 (2015) 90–95. https://doi.org/10.1016/j.porgcoat.2014.09.018.

[3] R.J. Tremont, D.R. Blasini, C.R. Cabrera, Controlled self-assembly of mercapto and silane terminated molecules at Cu surfaces, J. Electroanal. Chem. 556 (2003) 147–158. https://doi.org/10.1016/S0022-0728(03)00340-1.

[4] F. Zucchi, A. Frignani, V. Grassi, G. Trabanelli, M. DalColle, The formation of a protective layer of 3-mercapto-propyl-trimethoxy-silane on copper, Corros. Sci. 49 (2007) 1570–1583. https://doi.org/10.1016/j.corsci.2006.08.019.

[5] A. Balbo, A. Frignani, C. Monticelli, Influence of nanoparticles on the inhibiting efficiency of organosilane coatings on bronze. Part 1: Electrochemical characterization, in: Eurocorr 2012 (EFC Event n.330), EFC, London, UK (CD-ROM), Istanbul, Turkey, 2012: pp. 1-8 (Paper 1524).

[6] A. Balbo, C. Chiavari, C. Martini, C. Monticelli, Effectiveness of corrosion inhibitor films for the conservation of bronzes and gilded bronzes, Corros. Sci. 59 (2012) 204–212. https://doi.org/10.1016/j.corsci.2012.03.003.

[7] C. Chiavari, A. Balbo, E. Bernardi, C. Martini, F. Zanotto, I. Vassura, M.C. Bignozzi, C. Monticelli, Organosilane coatings applied on bronze: Influence of UV radiation and thermal cycles on the protectiveness, Prog. Org. Coatings. 82 (2015) 91–100. https://doi.org/10.1016/j.porgcoat.2015.01.017.

[8] C. Chiavari, A. Balbo, E. Bernardi, C. Martini, M.C. Bignozzi, M. Abbottoni, C. Monticelli, Protective silane treatment for patinated bronze exposed to simulated natural environments, Mater. Chem. Phys. 141 (2013) 502–511. https://doi.org/10.1016/j.matchemphys.2013.05.050.

[9] G. Masi, C. Josse, J. Esvan, C. Chiavari, E. Bernardi, C. Martini, M. Bignozzi, C. Monticelli, F. Zanotto, A. Balbo, E. Švara Fabjan, T. Kosec, L. Robbiola, Evaluation of the protectiveness of an organosilane coating on patinated Cu-Si-Mn bronze for contemporary art, Prog. Org. Coatings. 127 (2019) 286–299.

[10] M. Albini, C. Chiavari, E. Bernardi, C. Martini, L. Mathys, E. Joseph, Evaluation of the performances of a biological treatment on tin-enriched bronze, Environ. Sci. Pollut. Res. (2016) 1–10. https://doi.org/10.1007/s11356-016-7361-2.

[11] M. Albini, Fungal biogenic patina: optimization of an innovative conservation treatment for copper-based artefacts, University of Neuchatel, Swiss, 2017.

[12] G. Giuntoli, L. Rosi, M. Frediani, B. Sacchi, B. Salvadori, S. Porcinai, P. Frediani, Novel coatings from renewable resources for the protection of bronzes, Prog. Org. Coatings. 77 (2014) 892–903.

https://doi.org/10.1016/j.porgcoat.2014.01.021.

[13] F. Faraldi, E. Angelini, C. Riccucci, A. Mezzi, D. Caschera, S. Grassini, Innovative diamond-like carbon coatings for the conservation of bronzes, Surf. Interface Anal. 46 (2014) 764–770. https://doi.org/10.1002/sia.5367.

[14] J. Wolfe, R. Grayburn, A review of the development and testing of Incralac lacquer A review of the development and testing of Incralac lacquer, J. Am. Inst. Conserv. (2017) 1–20. https://doi.org/10.1080/01971360.2017.1362863.

[15] J. Kim, K. Chang, T. Isobe, S. Tanabe, Acute toxicity of benzotriazole ultraviolet stabilizers on freshwater crustacean (Daphnia pulex), J. Toxicol. Sci. 36 (2011) 247–251.

[16] D.L. Moffett, Wax coatings on ethnographic metal objects: Justifications for allowing a tradition to wane, J. Am. Inst. Conserv. 35 (1996) 1–7.

[17] C.A. Grissom, N. Grabow, C.S. Riley, A.E. Charola, Evaluation of coating performance on silver exposed to hydrogen sulfide, J. Am. Inst. Conserv. 52 (2013) 82–96.

[18] T. Jaeger, Short communication removal of paraffin wax in the re-treatment of archaeological iron, J. Am. Inst. Conserv. 47 (2008) 217–223.

[19] R.A. Iezzi, S. Gaboury, K. Wood, Acrylic-fluoropolymer mixtures and their use in coatings, Prog. Org. Coatings. 40 (2000) 55–60. https://doi.org/10.1016/S0300-9440(00)00117-X.

[20] B. Salvadori, A. Cagnini, M. Galeotti, S. Porcinai, S. Goidanich, A. Vicenzo, C. Celi, P. Frediani, L. Rosi, M. Frediani, G. Giuntoli, L. Brambilla, R. Beltrami, S. Trasatti, Traditional and innovative protective coatings for outdoor bronze : Application and performance comparison, J. Appl. Polym. Sci. 460112 (2017) 1–12. https://doi.org/10.1002/app.46011.

[21] G. Bierwagen, T.J. Shedlosky, K. Stanek, Developing and testing a new generation of protective coatings for outdoor bronze sculpture, Prog. Org. Coatings. 48 (2003) 289–296. https://doi.org/10.1016/j.porgcoat.2003.07.004.

[22] V.C. Malshe, N.S. Sangaj, Fluorinated acrylic copolymers: Part I: Study of clear coatings, Prog. Org. Coatings. 53 (2005) 207–211. https://doi.org/10.1016/j.porgcoat.2005.03.003.

[23] K. Satoh, H. Nakazumi, M. Morita, Preparation of super-water-repellent fluorinated inorganic-organic coating films on nylon 66 by the sol-gel method using microphase separation, J. Sol-Gel Sci. Technol. 27 (2003) 327–332. https://doi.org/10.1023/A:1024025104733.

[24] B. Baradie, M.S. Shoichet, Novel fluoro-terpolymers for coatings applications, Macromolecules. 38 (2005) 5560–5568. https://doi.org/10.1021/ma047792s.

[25] M. Sadat-Shojai, A. Ershad-Langroudi, Polymeric Coatings for Protection of Historic Monuments: Opportunities and Challenges, J. Appl. Polym. Sci. 112 (2009) 2535–2551. https://doi.org/10.1002/app.29801.

[26] T. Kosec, L. Škrlep, E. Švara Fabjan, A.S. Skapin, G. Masi, E. Bernardi, C. Chiavari, C. Josse, J. Esvan, L. Robbiola, Development of multi-component fluoropolymer based coating on simulated outdoor patina on quaternary bronze, Prog. Org. Coatings. 131 (2019) 27–35.

[27] G. Masi, M. Aufray, A. Balbo, E. Bernardi, M. Bignozzi, C. Chiavari, J. Esvan, N. Gartner, V. Grassi, C. Josse, T. Kosec, C. Martini, C. Monticelli, L. Škrlep, W. Sperotto, E. Švara Fabjan, E. Tedesco, F. Zanotto, L. Robbiola, B-IMPACT project: eco-friendly and non-hazardous coatings for the protection of outdoor bronzes, in: Accept. Publ. IOP Conf. Ser., 2020.

[28] M. Aufray, A. Balbo, F. Benetti, E. Bernardi, M. Bignozzi, C. Chiavari, J. Esvan, N. Gartner, V. Grassi, C. Josse, T. Kosec, C. Martini, G. Masi, C. Monticelli, L. Robbiola, L. Škrlep, W. Sperotto, E. Švara Fabjan, E. Tedesco, F. Zanotto, Protection of outdoor bronzes by eco-friendly and non-hazardous coatings based on silane and fluoropolymers: results from the B-IMPACT project, in: Proc. ICOM-CC Conf. Met. 2019, 2019.

[29] C. Chiavari, E. Bernardi, C. Martini, L. Morselli, F. Ospitali, L. Robbiola, A. Texier, Predicting the corrosion behaviour of outdoor bronzes: assessment of artificially exposed and real outdoor samples, Met. 2010 Proc. Interim Meet. ICOM-CC Met. Work. Group, Oct. 11-15, 2010, Charleston, South Carolina, USA. (2011) 218–226.

[30] E. Bernardi, C. Chiavari, B. Lenza, C. Martini, L. Morselli, F. Ospitali, L. Robbiola, The atmospheric corrosion of quaternary bronzes: The leaching action of acid rain, Corros. Sci. 51 (2009) 159–170. https://doi.org/10.1016/j.corsci.2008.10.008.

[31] G. Masi, J. Esvan, C. Josse, C. Chiavari, E. Bernardi, C. Martini, M.C. Bignozzi, N. Gartner, T. Kosec, L. Robbiola, Characterization of typical patinas simulating bronze corrosion in outdoor conditions, Mater. Chem. Phys. 200 (2017) 308–321. https://doi.org/10.1016/j.matchemphys.2017.07.091.

[32] C. Chiavari, K. Rahmouni, H. Takenouti, S. Joiret, P. Vermaut, L. Robbiola, Composition and electrochemical properties of natural patinas of outdoor bronze monuments, Electrochim. Acta. 52 (2007) 7760–7769. https://doi.org/10.1016/j.electacta.2006.12.053.

[33] P. Vazquez, L. Carrizo, C. Thomachot-Schneider, S. Gibeaux, F.J. Alonso, Influence of surface finish and composition on the deterioration of building stones exposed to acid atmospheres, Constr. Build. Mater. 106 (2016) 392–403.

[34] S. Goidanich, L. Toniolo, S. Jafarzadeh, I.O. Wallinder, Effects of wax-based anti-graffiti on copper patina composition and dissolution during four years of outdoor urban exposure, J. Cult. Herit. 11 (2010) 288–296.

[35] L. Graziani, E. Quagliarini, F. Bondioli, M. D'Orazio, Durability of self-cleaning TiO2 coatings on fired clay brick façades: Effects of UV exposure and wet & dry cycles, Build. Environ. 71 (2014) 193–203.

[36] S. Goidanich, J. Brunk, G. Herting, M.A. Arenas, I.O. Wallinder, Atmospheric corrosion of brass in outdoor applications: Patina evolution, metal release and aesthetic appearance at urban exposure conditions, Sci. Total Environ. 412 (2011) 46–57.

[37] C. Chiavari, E. Bernardi, A. Balbo, C. Monticelli, S. Raffo, M.C. Bignozzi, C. Martini, Atmospheric corrosion of fire-gilded bronze: corrosion and corrosion protection during accelerated ageing tests, Corros. Sci. 100 (2015) 435–447. https://doi.org/http://dx.doi.org/10.1016/j.corsci.2015.080.013.

[38] C. Chiavari, E. Bernardi, D. Cauzzi, S. Volta, M.C. Bignozzi, B. Lenza, S. Montalbani, L. Robbiola, C. Martini, Influence of natural patinas of outdoor quaternary bronzes on conservation treatments, Met. 2013 Proc. Interim Meet. ICOM-CC Met. Work. Gr. (2013) 159–168.

[39] C. Debiemme-Chouvy, F. Ammeloot, E.M.M. Sutter, X-ray photoemission investigation of the corrosion film formed on a polished Cu-13Sn alloy in aerated NaCl solution, Appl. Surf. Sci. 174 (2001) 55–61.

[40] L. Robbiola, J.M. Blengino, C. Fiaud, Morphology and mechanisms of formation of natural patinas on archeological Cu-Sn alloys, Corros. Sci. 40 (1998) 2083–2111.

[41] L. Robbiola, K. Rahmouni, C. Chiavari, C. Martini, D. Prandstraller, A. Texier, H. Takenouti, P. Vermaut, New insight into the nature and properties of pale green surfaces of outdoor bronze monuments, Appl. Phys. A Mater. Sci. Process. 92 (2008) 161–169. https://doi.org/10.1007/s00339-008-4468-4.

[42] M. Seah, The quantitative analysis of surfaces by XPS: A review, Surf. Interface Anal. 2 (1980) 222–239. https://doi.org/10.1002/sia.740020607.

[43] F. Sinapi, S. Julien, D. Auguste, L. Hevesi, J. Delhalle, Z. Mekhalif, Monolayers and mixed-layers on copper towards corrosion protection, Electrochim. Acta. 53 (2008) 4228–4238. https://doi.org/10.1016/j.electacta.2007.12.061.

[44] Y.S. Li, W. Lu, Y. Wang, T. Tran, Studies of (3-mercaptopropyl)trimethoxylsilane and bis(trimethoxysilyl)ethane sol-gel coating on copper and aluminum, Spectrochim. Acta - Part A Mol. Biomol. Spectrosc. 73 (2009) 922–928. https://doi.org/10.1016/j.saa.2009.04.016.

[45] G. Masi, A. Balbo, J. Esvan, C. Monticelli, J. Avila, L. Robbiola, E. Bernardi, M.C. Bignozzi, M.C. Asensio, C. Martini, C. Chiavari, X-ray Photoelectron Spectroscopy as a tool to investigate silane-based coatings for the protection of outdoor bronze: The role of alloying elements, Appl. Surf. Sci. 433 (2018). https://doi.org/10.1016/j.apsusc.2017.10.089.

[46] N. Cioffi, N. Ditaranto, L. Torsi, R.A. Picca, L. Sabbatini, A. Valentini, L. Novello, G. Tantillo, T. Bleve-Zacheo, P.G. Zambonin, Analytical characterization of bioactive fluoropolymer ultra-thin coatings modified by copper nanoparticles, Anal. Bioanal. Chem. 381 (2005) 607–616. https://doi.org/10.1007/s00216-004-2761-4.

[47] F. Sinapi, J. Delhalle, Z. Mekhalif, XPS and electrochemical evaluation of two-dimensional organic films obtained by chemical modification of self-assembled monolayers of (3-mercaptopropyl) trimethoxysilane on copper surfaces, Mater. Sci. 22 (2002) 345–353. https://doi.org/10.1016/S0928-4931(02)00210-2.

[48] A. Galtayries, A. Mongiatti, P. Marcus, C. Chiavari, Surface characterisation of corrosion inhibitors on bronzes for artistic casting, Corros. Met. Herit. Artefacts Investig. Conserv. Predict. Long Term Behav. 48 (2007) 335–351. https://doi.org/10.1533/9781845693015.335.

[49] P.M. Dietrich, S. Glamsch, C. Ehlert, A. Lippitz, N. Kulak, W.E.S. Unger, Synchrotron-radiation XPS analysis of ultra-thin silane films : Specifying the organic silicon, Appl. Surf. Sci. 363 (2016) 406–411.

[50] M. Finšgar, 2-Mercaptobenzimidazole as a copper corrosion inhibitor: Part II. Surface analysis using X-ray photoelectron spectroscopy, Corros. Sci. 72 (2013) 90–98. https://doi.org/10.1016/j.corsci.2013.03.010.

[51] Z. Mekhalif, L. Massi, F. Guittard, S. Geribaldi, J. Delhalle, X-Ray photoelectron spectroscopy study of polycrystalline zinc modified by n -dodecanethiol and 3-perfluorooctyl-propanethiol, 405 (2002) 186–193.

[52] F. Sinapi, I. Lejeune, J. Delhalle, Z. Mekhalif, Comparative protective abilities of organothiols SAM coatings applied to copper dissolution in aqueous environments, Electrochim. Acta. 52 (2007) 5182–5190. https://doi.org/10.1016/j.electacta.2006.12.087.

[53] G. Wyszecki, W.S. Stiles, Color science: concepts and methods, quantitative data and formulas, (1982).

FIGURE CAPTIONS

Figure 1: Free surfaces of (a) patinated bronze sample and (b) FA-MS coating on patinated bronze observed by SEM.

Figure 2: Field test of the bronze statue representing the Slovenian poet France Prešeren in outdoor exposition in the park of ZAG Institute (Slovenia), initially corroded during one year in urban environment. FA-MS coated corroded statue before (left) and after 9 months (right) of natural outdoor exposure.

Figure 3: Surface observation of uncoated bronze after accelerated ageing by dropping test (10 days of ToW): (a) optical microscopy image; (b) back scattered electron (BE) image (c) EDS X-ray maps (BE image, O-K, Cu-L, Zn-L, Sn-L and Pb-M).

Figure 4: FIB cross-section observation of uncoated patinated bronze after ageing by dropping test: (a) general view of a corroded dendrite with an eutectoid area with corrosion layer produced by ageing; (b and c) details of the corrosion layer in the dendrite border (b) and in the dendrite core (c) revealing variable thicknesses (b and c) and densities (d and e); (f) EDS X-ray maps of a representative portion of the cross-section with the eutectoid in the centre of the image (Electron image, O-K, Cu-L, Zn-L, Sn-L and Pb-M).

Figure 5: Mass variation for the uncoated (black diamonds) and FA-MS coated patinated bronze (orange dots) during accelerated ageing by dropping.

Figure 6: FIB cross-sections of FA-MS coated bronze after ageing by dropping: (a and b) images of the FA-MS layer at different magnifications; (c) EDS maps of a representative portion of cross-section (C-K, O-K, F-K, Si-K, Cu-L,Sn-L and Pt-M).

Figure 7: Optical micrographs comparing the different cleaning methods applied on the FA-MS in as-coated (top) and coated after ageing (bottom) conditions, with surface roughness profiles (Rq value) on the right. The Rq value is also reported in Table 3.

Figure 8: Back-scattered SEM micrographs of the coated surfaces before and after the different cleaning procedures. Images are reported for coated patinated bronze samples both before and after the accelerated ageing.

Figure 9: EDS data of the as-coated samples and coated ones after ageing when blasting and brushing (using nylon and steel brushes) are applied: (a, c) characteristic elements of FA-MS (C, O, F and Si) and (b, d) alloying elements (Cu, Zn, Sn and Pb) are reported.

Figure 10: Py-GC-MS chromatograms of the residues scraped off equal spots of the following surfaces: (a) as-coated, (b) as-coated and cleaned by nylon brush, (c) as-coated and cleaned by steel brush.

TABLE CAPTIONS

Table 1: Cumulative metallic ions release (Cu, Pb and Zn) in $\mu g/cm^2$ with standard deviation values (sd), from patinated bronze (uncoated or coated by FA-MS) in the synthetic acid rain solution, as a function of exposure time (dropping test). Zn ions in the weathering solutions of the FA-MS coated bronze were under the Limit of Detection ($LoD_{Zn} = 20\ \mu g/cm^2$).

Table 2: XPS data of the different chemical species detected on the FA-MS surface before and after dropping test.

Table 3: XRF results with the standard deviation values (sd) of the three measuring points in the “before” and “after” conditions (Figure. 2), representative of 9 months of natural outdoor exposure.

Table 4: Surface roughness (Ra and Rq) induced by the three selected cleaning methods, obtained on the as-coated patinated samples and after accelerated ageing. Standard deviation values (sd) are reported.

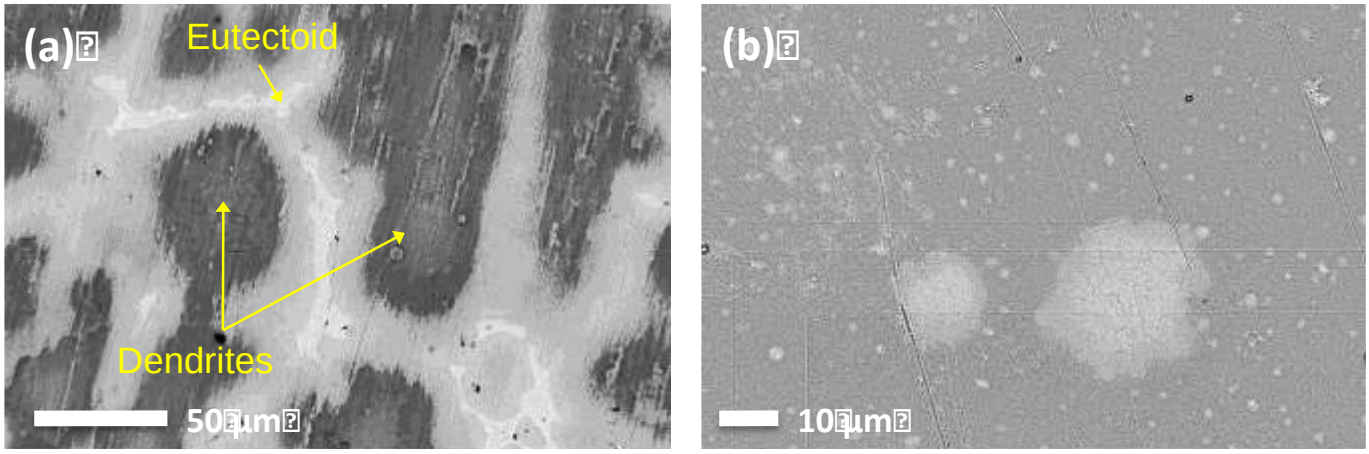

Figure 1: Free surfaces of (a) patinated bronze sample and (b) FA-MS coating on patinated bronze observed by SEM.

BEFORE AGEING (April 2018) AFTER AGEING (January 2019)

Figure 2: Field test of the bronze statue representing the Slovenian poet France Prešeren in outdoor exposition in the park of ZAG Institute (Slovenia), initially corroded during one year in urban environment. FA-MS coated corroded statue before (left) and after 9 months (right) of natural outdoor exposure.

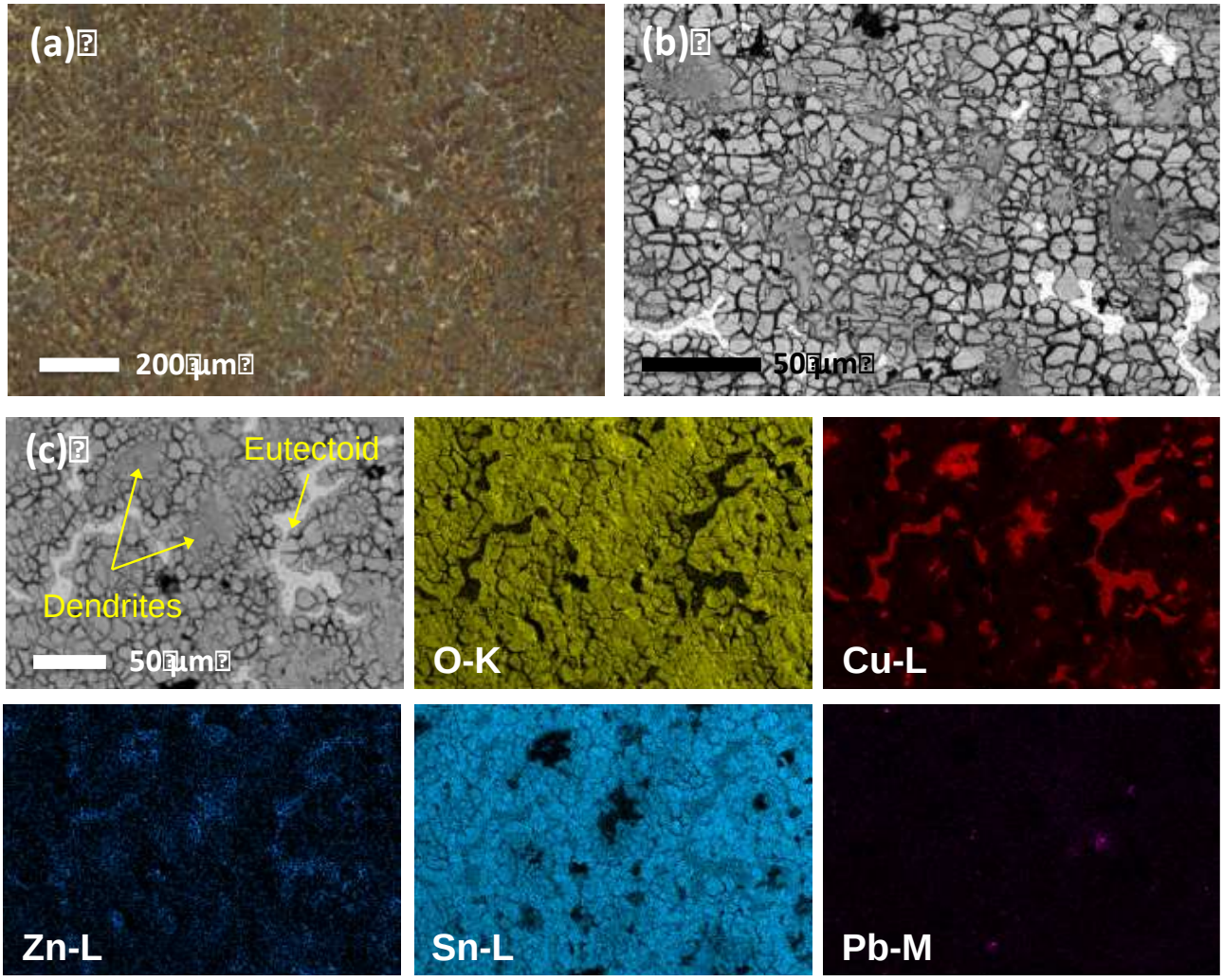

Figure 3: Surface observation of uncoated bronze after accelerated ageing by dropping test (10 days of ToW): (a) optical microscopy image; (b) back scattered electron (BE) image (c) EDS X-ray maps (BE image, O-K, Cu-L, Zn-L, Sn-L and Pb-M).

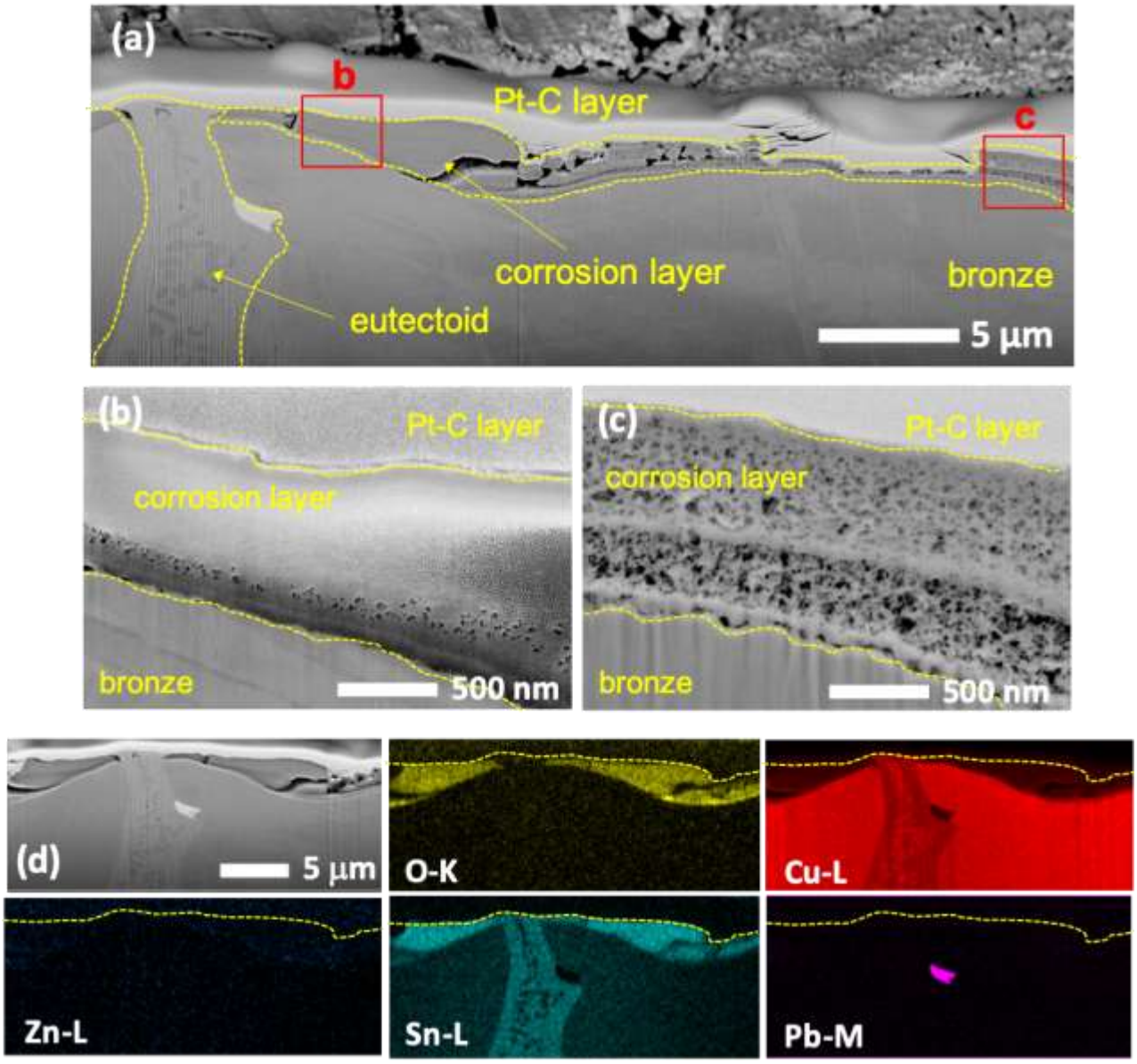

Figure 4: FIB cross-section observation of uncoated patinated bronze after ageing by dropping test: (a) general view of a corroded dendrite with an eutectoid area with corrosion layer produced by ageing; (b and c) details of the corrosion layer in the dendrite border (b) and in the dendrite core (c) revealing variable thicknesses (b and c) and densities (d and e); (f) EDS X-ray maps of a representative portion of the cross-section with the eutectoid in the centre of the image (Electron image, O-K, Cu-L, Zn-L, Sn-L and Pb-M).

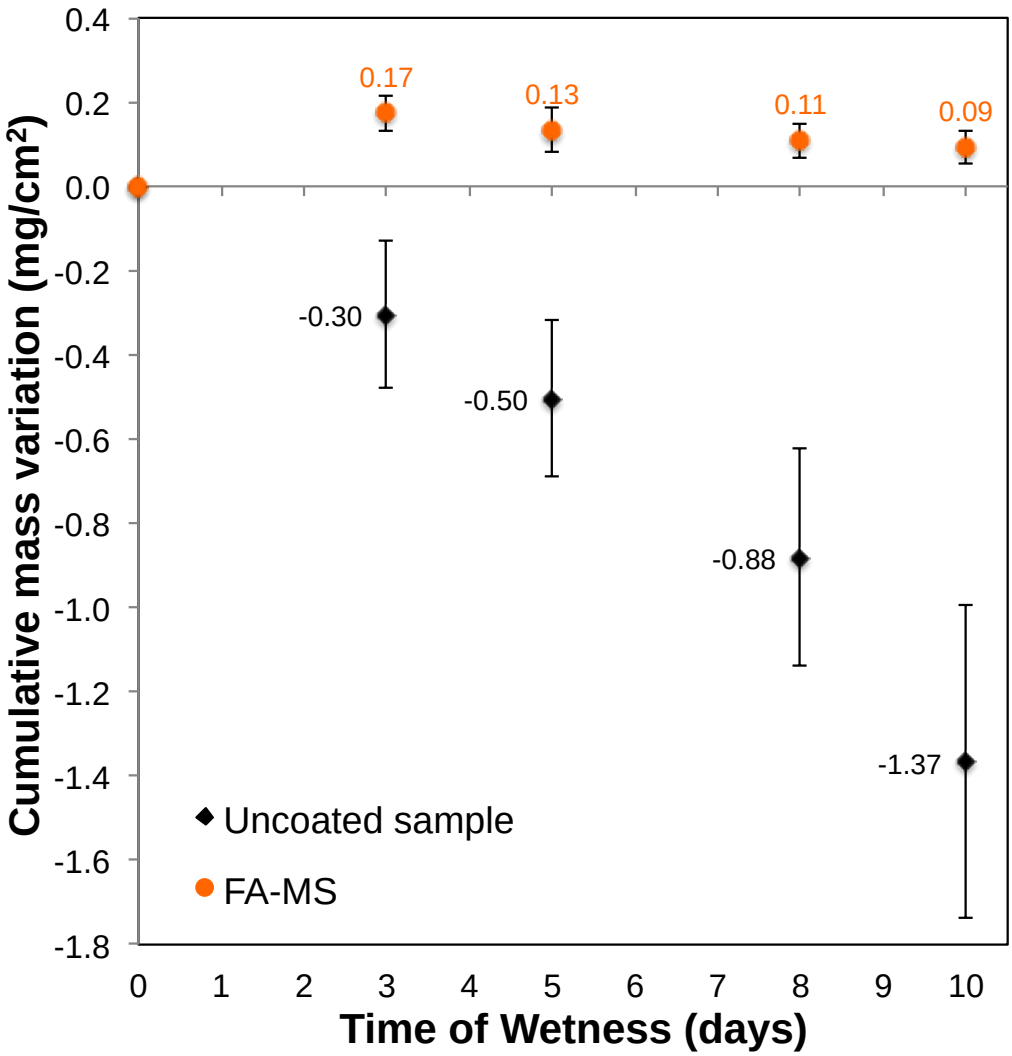

Figure 5: Mass variation for the uncoated (black diamonds) and FA-MS coated patinated bronze (orange dots) during accelerated ageing by dropping.

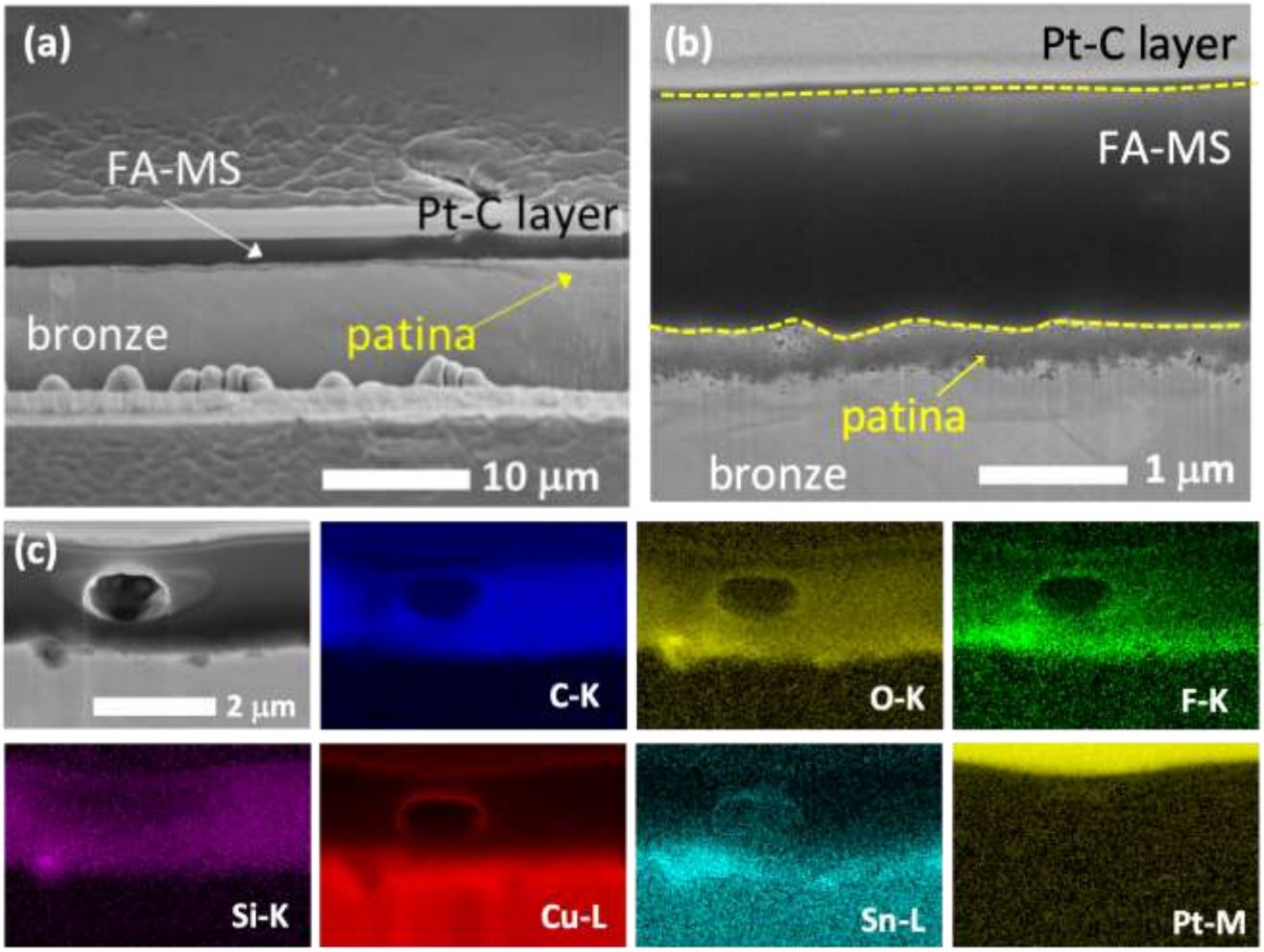

Figure 6: FIB cross-sections of FA-MS coated bronze after ageing by dropping: (a and b) images of the FA-MS layer at different magnifications; (c) EDS maps of a representative portion of cross-section (C-K, O-K, F-K, Si-K, Cu-L,Sn-L and Pt-M).

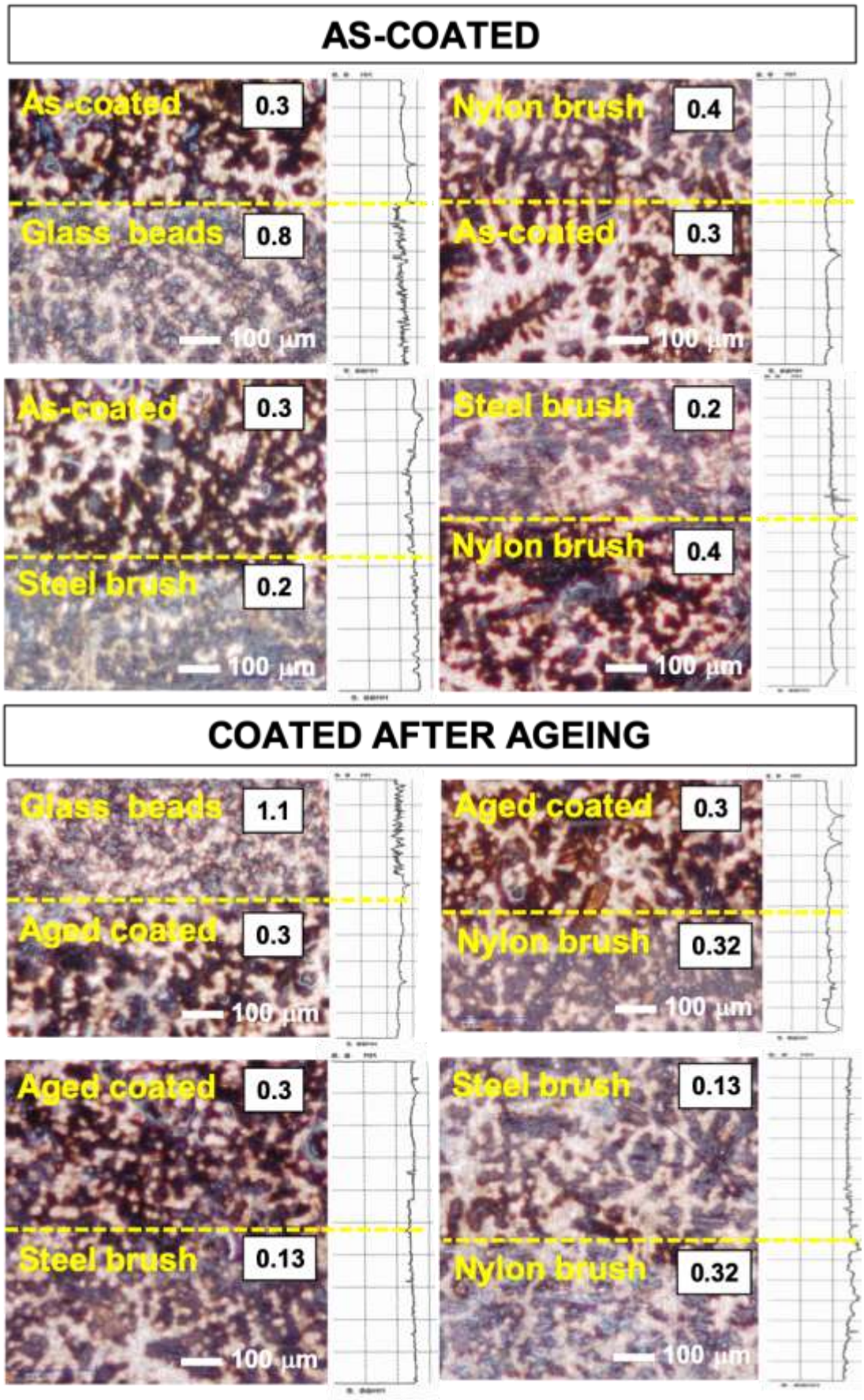

Figure 7: Optical micrographs comparing the different cleaning methods applied on the FA-MS in as-coated (top) and coated after ageing (bottom) conditions, with surface roughness profiles (Rq value) on the right. The Rq value is also reported in Table 3.

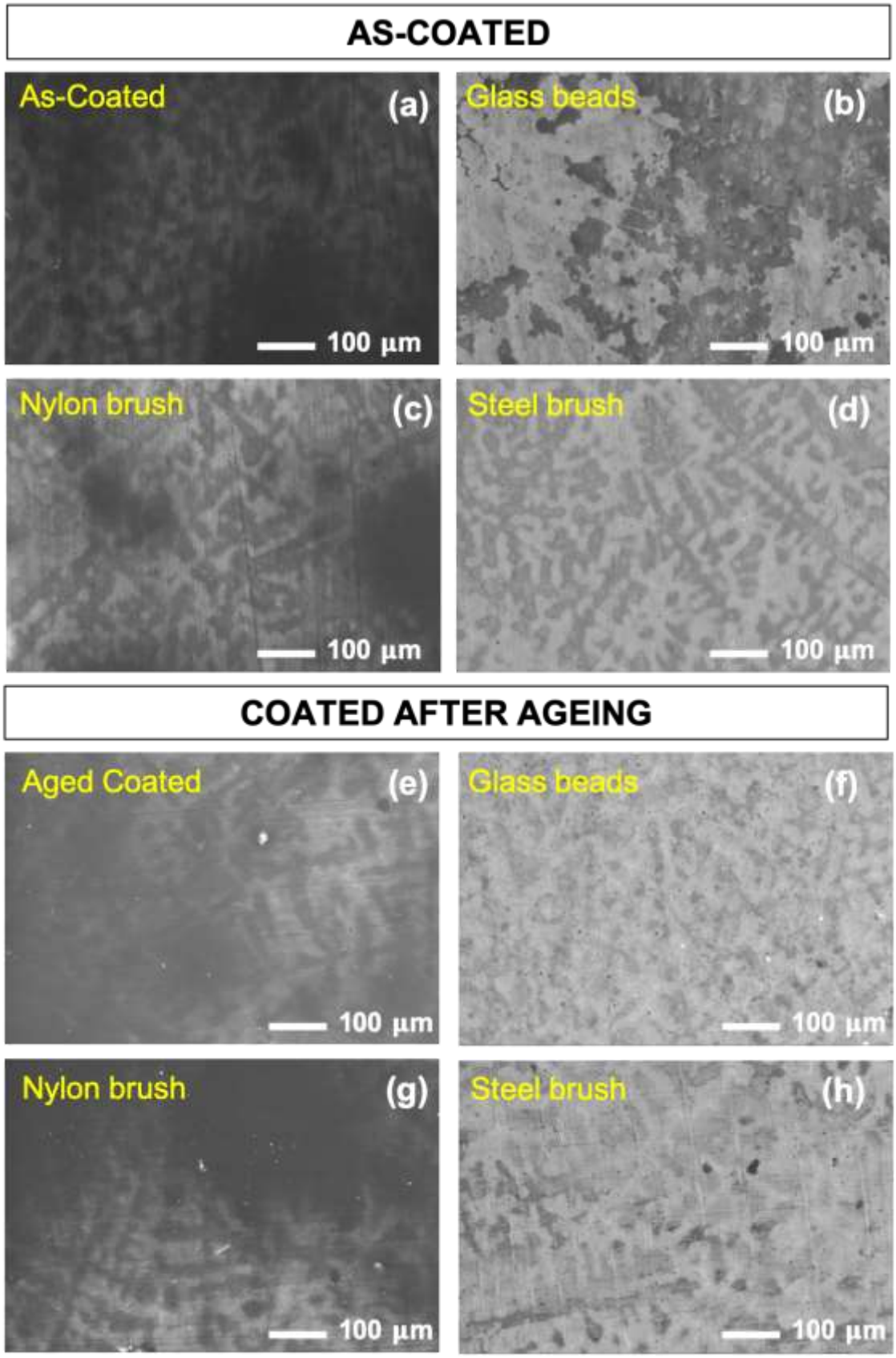

Figure 8: Back-scattered SEM micrographs of the coated surfaces before and after the different cleaning procedures. Images are reported for coated patinated bronze samples both before and after the accelerated ageing.

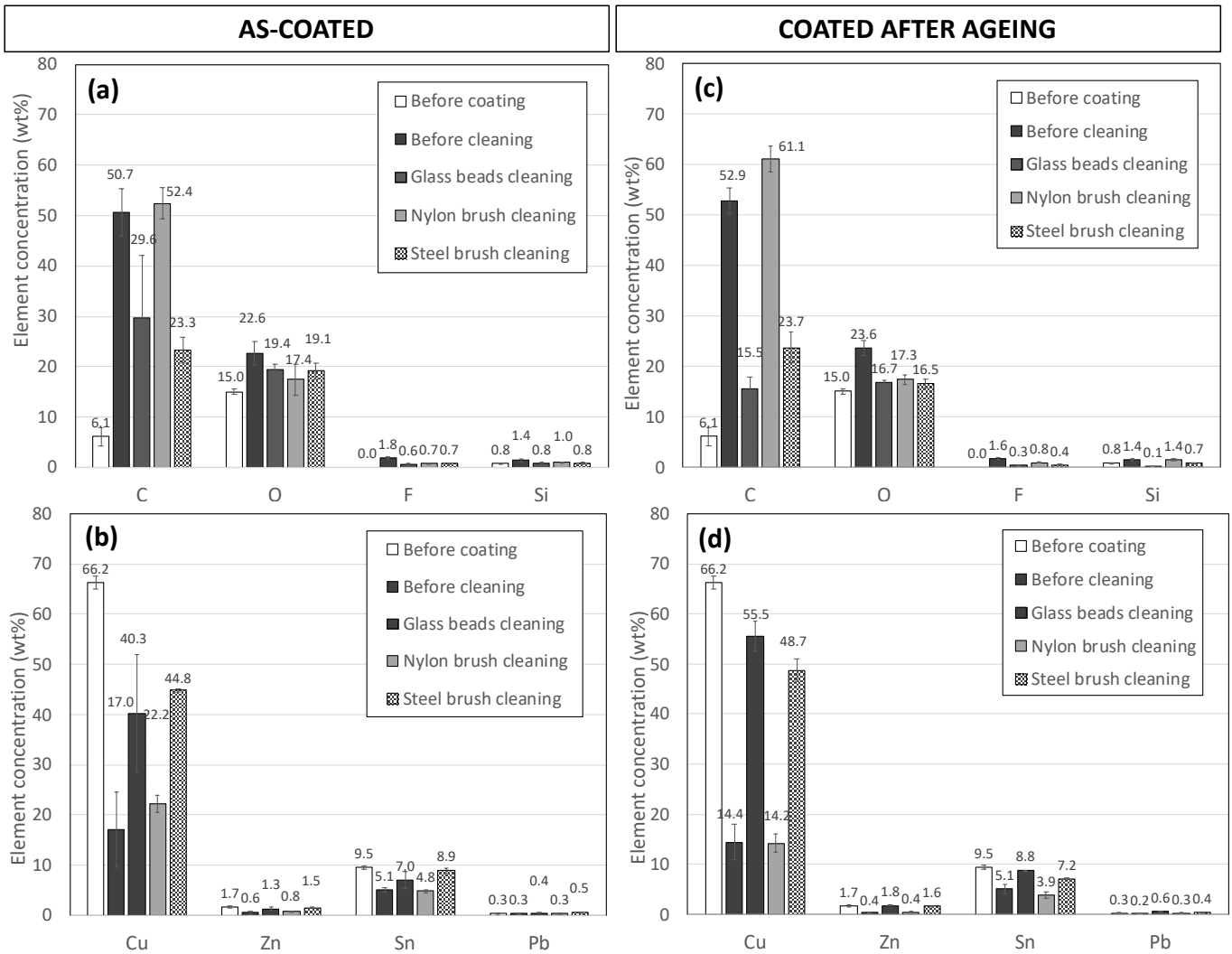

Figure 9: EDS data of the as-coated samples and coated ones after ageing when blasting and brushing (using nylon and steel brushes) are applied: (a, c) characteristic elements of FA-MS (C, O, F and Si) and (b, d) alloying elements (Cu, Zn, Sn and Pb) are reported.

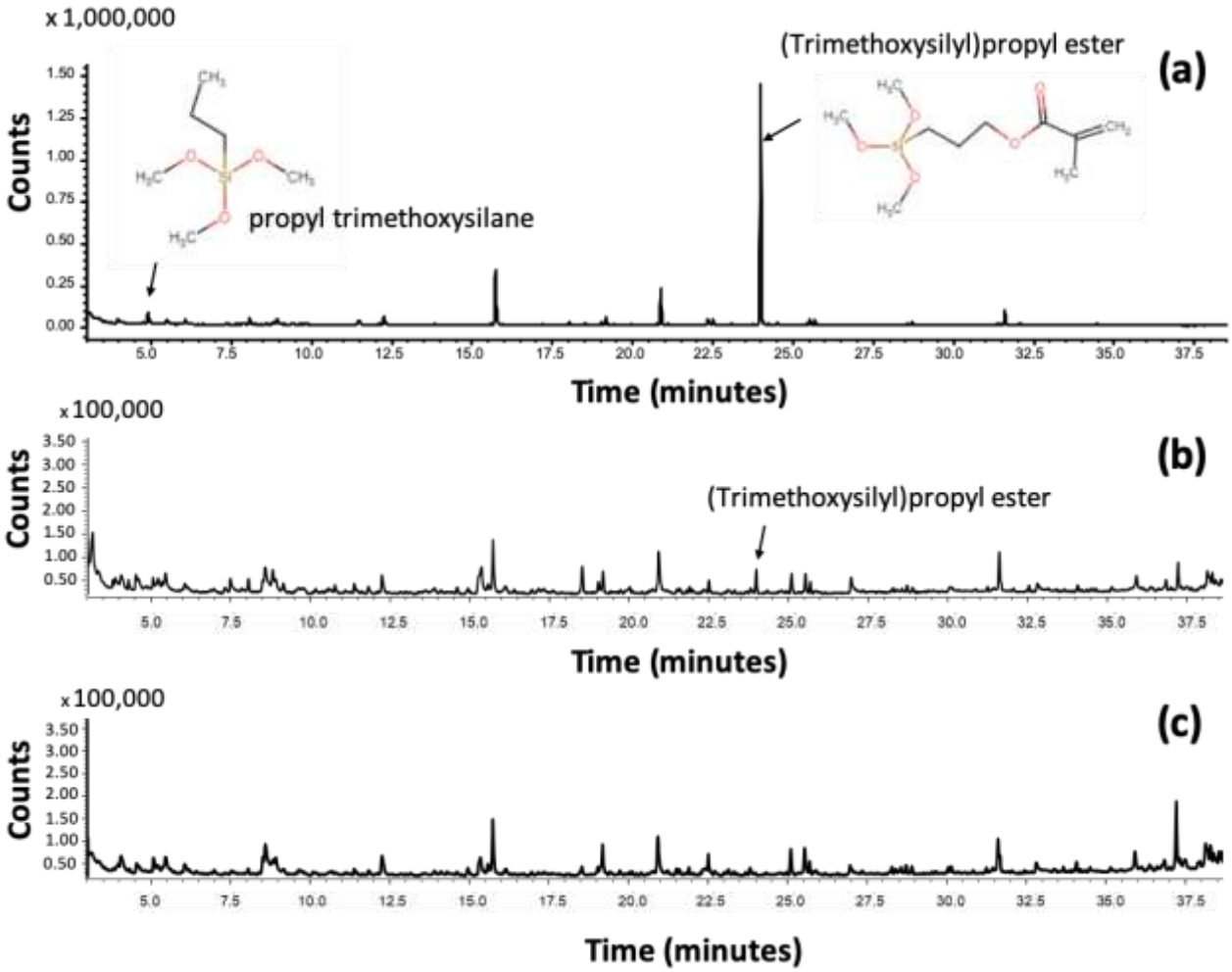

Figure 10: Py-GC-MS chromatograms of the residues scraped off equal spots of the following surfaces: (a) as-coated, (b) as-coated and cleaned by nylon brush, (c) as-coated and cleaned by steel brush.

Table 1: Cumulative metallic ions release (Cu, Pb and Zn) in μg/cm² with standard deviation values (sd), from patinated bronze (uncoated or coated by FA-MS) in the synthetic acid rain solution, as a function of exposure time (dropping test). Zn ions in the weathering solutions of the FA-MS coated bronze were under the Limit of Detection (LoD_{Zn} = 20 μg/cm²).

	Time of Wetness, days											
Cumulative ions release, μg/cm²	**3**			**5**			**8**			**10**		
	Cu	**Zn**	**Pb**	**Cu**	**Zn**	**Pb**	**Cu**	**Zn**	**Pb**	**Cu**	**Zn**	**Pb**
Patinated bronze, uncoated	*429*	*23*	*54*	*718*	*36*	*67*	*1167*	*59*	*80*	*1617*	*81*	*94*
sd	*66*	*1*	*9*	*134*	*2*	*10*	*222*	*5*	*12*	*255*	*6*	*14*
Patinated bronze, FA-MS coated	*3.2*	*<LoD*	*0.23*	*5.6*	*<LoD*	*0.34*	*8.4*	*<LoD*	*0.39*	*12.0*	*<LoD*	*0.5*
sd	*1.3*	*-*	*0.01*	*2.1*	*-*	*0.01*	*1.6*	*-*	*0.01*	*0.6*	*-*	*0.1*

Table 2: XPS data of the different chemical species detected on the FA-MS surface before and after dropping test.

Element	Peak	Position (eV)	References	Before ageing (at%)	After ageing (at%)
C 1s	CC, CH, C-Si-O	284.7	[43–47]	40.7	47.8
	C-O, C-N	285.7-286-3		13.4	12.3
	C=O, O=C-O	287.1-289.0		4.1	4.6
	CF_2	291.4		5.2	4.4
	CF_3	293.8		1.5	1.4
N 1s	N-C	400.0	[48]	3.3	2.7
O 1s	O-Si, O-C	532.8	[43,47]	16.2	15.3
F 1s	F_x-C	684.3-688.7	[46]	13.3	9.0
Si 2p	C-Si-O, Si-O-Si	101.9	[43,44,47,49]	< 0.1	0.3
S $2p_{3/2}$	S-C, S-metal	163.2	[43,44,50–52]	-	0.2
	sulfates	168.8		2.4	1.8

Table 3: XRF results with the standard deviation values (sd) of the three measuring points in the "before" and "after" conditions (Figure. 2), representative of 9 months of natural outdoor exposure.

wt%	**Cu**	**Sn**	**Pb**	**Zn**	**Fe**	**Sn/Cu**
			Right shoulder (A)			
before	86.5	5.90	1.3	5.50	0.30	0.07
sd	0.6	0.09	0.4	0.02	0.01	-
after	86.6	6.10	1.4	5.5	0.29	0.07
sd	0.2	0.08	0.1	0.1	0.02	-
			Left shoulder (B)			
before	86.1	6.70	1.4	5.20	0.26	0.08
sd	0.6	0.09	0.4	0.02	0.01	-
after	87.0	5.70	1.2	5.6	0.27	0.07
sd	0.2	0.08	0.1	0.1	0.02	-
			Top of the head (C)			
before	86.6	6.30	1.4	5.20	0.35	0.07
sd	0.6	0.09	0.4	0.02	0.01	-
after	85.9	7.10	1.4	5.1	0.34	0.08
sd	0.2	0.08	0.1	0.1	0.02	-

Table 4: Surface roughness (Ra and Rq) induced by the three selected cleaning methods, obtained on the as-coated patinated samples and after accelerated ageing. Standard deviation values (sd) are reported.

	AS COATED				**COATED AFTER ACCELERATED AGEING**			
	Before cleaning	**Glass beads cleaning**	**Nylon brush cleaning**	**Steel brush cleaning**	**Before cleaning**	**Glass beads cleaning**	**Nylon brush cleaning**	**Steel brush cleaning**
Ra (μm)	0.21	0.6	0.2	0.17	0.17	0.9	0.21	0.09
sd	0.04	0.1	0.1	0.08	0.08	0.3	0.03	0.04
Rq (μm)	0.3	0.8	0.4	0.2	0.3	1.1	0.32	0.13
sd	0.1	0.1	0.2	0.1	0.1	0.5	0.07	0.07